IEEE Access
Multidisciplinary ⋮ Rapid Review ⋮ Open Access Journal

Received 17 December 2024, accepted 2 January 2025, date of publication 3 January 2025, date of current version 14 January 2025.

Digital Object Identifier 10.1109/ACCESS.2025.3525953

RESEARCH ARTICLE

Research on the Evolution Mechanism of Partial Discharge Signals for Arcing Faults in Transformers

CHENLEI HAN[1], KELI GAO[1,2], WENZHI CHANG[1], BO QI[3], JIANGANG BI[1], SHUAI YUAN[1], MENG HUANG[3], AND TINGYU GAO[1]

[1]China Electric Power Research Institute, Haidian, Beijing 100192, China
[2]State Key Laboratory of Power Grid Environmental Protection, Wuhan, Hubei 430072, China
[3]State Key Laboratory of Alternate Electrical Power System with Renewable Energy Sources, North China Electric Power University, Changping, Beijing 102206, China

Corresponding author: Chenlei Han (hanchenlei@epri.sgcc.com.cn)

This work was supported by the Science & Technology Project of State Grid Corporation of China under Grant 5500-202155418A-0-0-00.

ABSTRACT Effective monitoring and identification of partial discharge (PD) signals caused by arcing faults is essential for the prevention of transformer explosions. However, there is still a deficiency in the comprehension of the evolution of PD signals resulting from arcing faults. This study investigated the characteristics of PD signals, including electricity, sound, and pressure, during arc discharge through transformer arc discharge experiments. During the experiment, the ultra-high frequency (UHF) electromagnetic PD signal excited by arc discharge demonstrated good continuity, yet the amplitude of the pulse signal was low. The high-frequency current PD signal merely generates a pulse signal at the instant of arc initiation. The mediate-frequency current PD signal emerges in the form of periodic pulse signals. The amplitude of the low-frequency current PD signal is the highest and shows a continuous periodic pattern. Additionally, arc discharge leads to rapid pressure variations accompanied by audible and ultrasonic signals. The experimental results bridge the gap in the study of the PD signal characteristics during arc discharge in transformers, offering data support for the identification and early warning of transformer arcing faults.

INDEX TERMS Transformer, arc discharge, condition monitoring, sensors.

I. INTRODUCTION

Transformers play a pivotal role as the essential core equipment in ultra-high voltage power transmissions. Due to factors such as insulation deterioration and manufacturing process defects, the insulation performance of key parts such as windings in transformers will decrease during long-term operation, leading to local discharge defects in insulation. The occurrence of partial discharge defects within the transformer has the potential to result in degradation of the winding insulation structure, and in extreme instances, may even precipitate catastrophic events such as explosions. When the internal insulation structure of the transformer discharges, it is commonly accompanied by a variety of characteristic signals including electrical, magnetic, thermal, and acoustic [1]. Monitoring these insulation discharge signals enables effective identification and evaluation of transformer defects. This has significant practical implications for achieving early warning of transformer faults and preventing explosion accidents.

Current research suggests that internal insulation defects in large oil-filled equipment, such as transformers, typically progress through three stages of development: early local partial discharge, midterm local spark discharge, and late-stage penetrating arc discharge [2], [3]. Presently, research on online monitoring technology for transformer faults primarily focuses on the early and mid-term fault development by enhancing the absolute sensitivity of the sensor monitoring system to detect weak PD signals at an earlier stage. Previous studies [4], [5] have proposed a design concept for

The associate editor coordinating the review of this manuscript and approving it for publication was Arpan Kumar Pradhan.

utilizing built-in UHF sensors to monitor PD signals within transformers, thereby improving the sensitivity of UHF sensors. Through continuous improvement of the calibration method [6] and interference suppression methods [7] for UHF PD signals, related research has revealed the characteristics of UHF PD signals in the early development of typical insulation defects under laboratory conditions [8]. Simultaneously, as fiber optic sensing technology advances, integrated fiber optic acoustic sensors are increasingly being considered as a viable option for monitoring transformer faults [9], [10]. Research [11], [12] has demonstrated that fiber optic ultrasonic sensing systems utilizing various sensing principles exhibit greater sensitivity in detecting PD signals in oil compared to traditional Lead Zirconate Titanate (PZT) sensing systems. Furthermore, relevant studies delve into the characteristic patterns of ultrasonic PD signals in typical transformer defects through a fiber optic sensing array system [13], and propose a high-precision positioning method for internal faults of transformer [14], [15]. In conclusion, advancements in the sensitivity of sensing systems such as UHF sensors and acoustic sensors have provided a preliminary understanding of the characteristic features of PD signals at the initial stage of typical defects in transformers [16], [17]. However, due to limitations such as experimental conditions, existing transformer fault monitoring often overlooks related research on arcing discharge stages during insulation breakdown. Reports on the characteristics of PD signals in the arcing discharge stage of transformer faults are still lacking, while continuous discharge of arcing inside transformers leading to sudden pressure increase is a direct cause of explosion accidents [18], [19]. Therefore, it is crucial to study and comprehend the evolution laws of PD signal characteristics in the arcing discharge stage, which is of great significance for accurate identification of arcing faults and rapid interruption of explosion accidents.

This study is conducted using an arcing fault test platform, which has been adapted from the structure of an actual transformer oil tank. By incorporating internal UHF sensors, acoustic sensors, and pressure wave sensors, as well as external grounding current sensors to monitor various PD signals including electrical, magnetic, acoustic, and pressure during arcing events. The research aims to investigate the evolutionary patterns of multiple characteristics of arc signals during arcing faults in transformers. This will contribute valuable practical insights for monitoring and early detection of arcing discharge faults in transformers.

II. EXPERIMENTAL SETUP

A. EXPERIMENTAL CIRCUIT SETTING

The circuit depicted in Figure 1 serves as the equivalent triggering mechanism for arcing discharge during the test, comprising a generator, a voltage regulator transformer, and an arcing system. The arcing system encompasses an oil tank, a transformer lifting base, a high-voltage casing, and

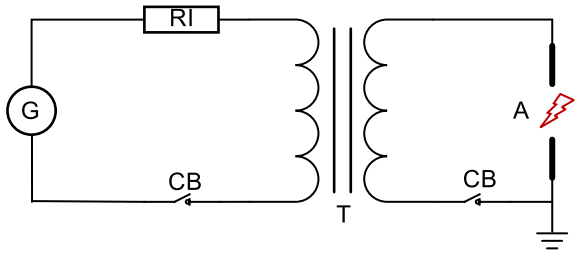

G-Generator; CB-Circuit Breaker; RI-Voltage Regulator Impedance; T-Voltage Regulator Transformer; A-Arc Initiation Device

FIGURE 1. Schematic diagram of equivalent circuit for arcing test.

an arc initiation device located within the tank as illustrated in Figure 2. Throughout the test procedure, AC high-voltage power at the required frequency is generated by the generator and voltage regulator transformer to be applied to the high-voltage electrode of the arcing device for initiating sustained arcing discharge. In this experiment, the arc duration was set at 80ms, which was determined in light of the fact that the transformer fault in the power system is usually cut off within 4 power cycles (50 Hz). Current transformers and voltage transformers are incorporated into the test circuit to capture and document data pertaining to both voltage and current levels of the arc throughout testing. The dimensions of the transformer oil tank utilized in the experiment are $4.5 \times 1.2 \times 1.4$ m, while the lifting base stands at a height of 3.3 m with a diameter of 1.1 m. The transformer is filled with transformer oil, of which the freezing point is 25°C. The high-voltage copper electrodes employed in the arc ignition device are all rod-shaped with a diameter measuring 10 mm, and there exists a gap of 200 mm between the high-voltage electrode and the ground electrode. The distance between the two electrodes was ascertained based on a specific transformer explosion fault. To ensure the formation of an arc discharge between the high-voltage copper electrodes, a copper arc initiation wire with a diameter of 1mm is employed to connect the electrodes [20]. Once the power circuit is

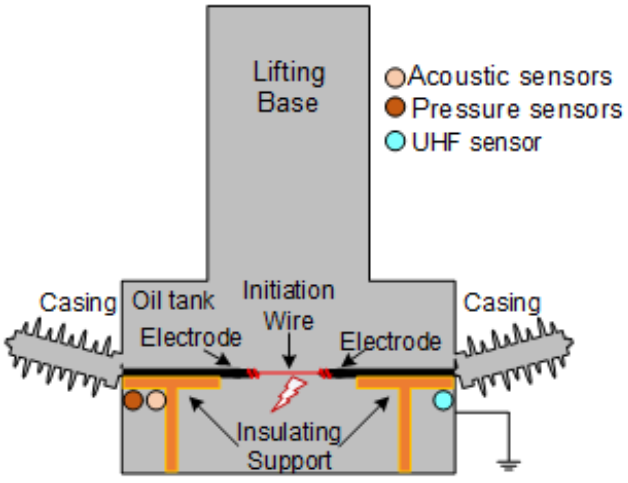

FIGURE 2. Schematic diagram of arc initiation system.

closed, the current can promptly melt the initiation wire to form an arc, thereby triggering the arc discharge fault that occurs during actual operation. Furthermore, an explosion-proof membrane device has been installed at the apex of the oil tank to ensure that internal pressure remains within mechanical strength limits during experimentation; it is worth noting that this device activates at a rated pressure of 50 kPa to prevent any potential overpressure situations from occurring.

B. SENSOR SETTINGS

The experiment was conducted with the installation of a UHF sensor, grounding current sensor, as well as fiber optic acoustic and pressure sensors to capture the variations in multiple arc signals including electrical, magnetic, acoustic, and pressure resulting from the arcing process. The arrangement of sensors is shown in Figure 3. To effectively acquire PD signals, sensors have been installed as close as possible to the arc discharge position while guaranteeing sensor safety. To tackle the problem of external interference, this experiment was conducted in a relatively enclosed setting, thereby effectively controlling the ambient noise factors.

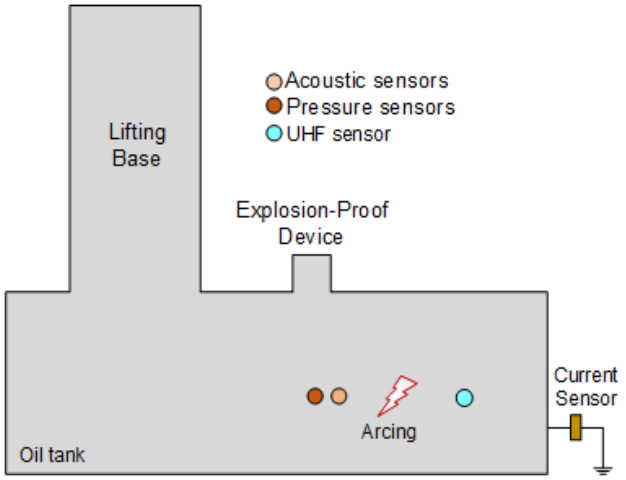

FIGURE 3. Schematic diagram of sensor arrangement.

The UHF sensor is utilized for continuous monitoring of UHF electromagnetic signals during the arcing process. The detection frequencies of the UHF sensor range from 300 MHz to 2 GHz, with an effective height of 12 mm. The sampling rate of the UHF sensor is 3 Gs/s. Positioned via a flange interface on the side wall of the oil tank near the arcing point, its sensing unit is housed inside the oil tank and oriented towards the arcing electrode at a distance of approximately 0.8 m.

The grounding current sensor is utilized for monitoring changes in ground current signal during the arcing process. The sensor has the capability to independently measure PD signals of high frequency, medium frequency, and low frequency, with detection bandwidths of 1 MHz∼30 MHz, 10 kHz∼1 MHz, and 40 Hz∼1 kHz respectively. It is connected to the grounding lead of the test device. The sampling rate of the grounding current sensor is 100 Ms/s.

Fiber optic acoustic sensors and pressure sensors detect the sound signal and pressure changes within the oil tank during the combustion process by demodulating the wavelength variation of fiber optic gratings [21]. The fiber optic sensing unit is integrated into the oil tank through a fiber penetrator on the side wall, secured to an insulating bracket of the arc ignition device as depicted in Figure 2, ensuring that both pressure sensing unit and sound sensing unit are oriented toward the arc point. The distance between fiber optic acoustic sensor and pressure sensor to the arc point is approximately 0.8m. The calibration detection frequency band of fiber optic acoustic sensor ranges from 5 kHz to 150 kHz, while for fiber optic pressure sensor, it covers a calibration pressure detection range of ±100 MPa. The sampling rate of the acoustic sensor is 1 Ms/s, which is 5 ks/s for the pressure sensor.

III. EXPERIMENTAL RESULTS AND DISCUSSION

A. ARCING PROCESS

To eliminate the occasional occurrence of a single experiment, the arc discharge test was conducted a total of 4 times. Despite the inherent randomness associated with arc discharge, the resulting arc signals exhibit strong common characteristics. This article is dedicated to analyzing and discussing the common characteristics of internal arcing faults in transformers.

Figure 4 illustrates the arc voltage and arc current excited by the arcing device. The arc current exhibits a sinusoidal waveform with a frequency of 50 Hz, consistent with the test system's current frequency. The amplitude of the arc current fluctuates between −38.7∼46.8 kA. Meanwhile, the arc voltage displays typical arcing waveform characteristics: upon closure of the circuit breaker, high voltage is applied between the arcing electrodes, leading to a rapid increase in voltage and breakdown of the inter-electrode oil gap to

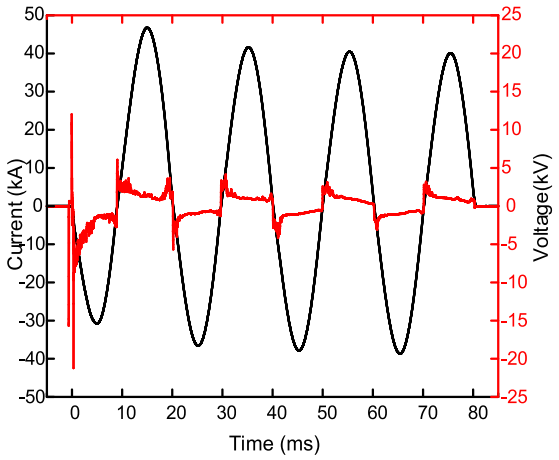

FIGURE 4. Voltage and current variation during arcing process.

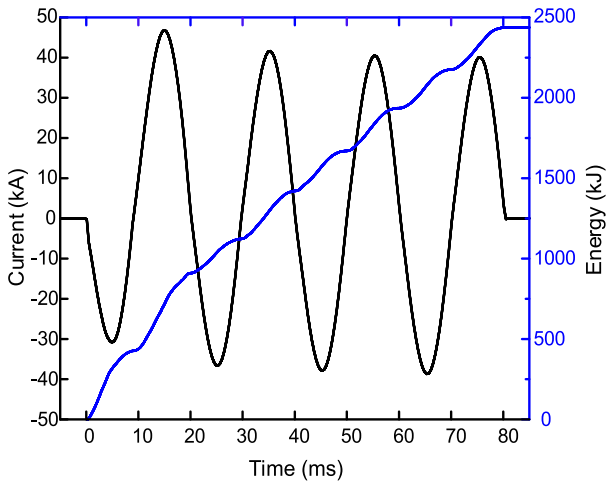

FIGURE 5. Arc energy variation during arcing process.

generate high-voltage arcs. The steady-state amplitude of the arc voltage fluctuates between −9.7∼8.4 kV throughout an approximately 80 ms total duration for the entire arcing process.

During the experimental procedure, the energy discharged by the arc can be computed based on the arc voltage and current data. The formula for determining arc energy is as follows (1):

$$W = \int_0^t |u_t \cdot i_t| dt \tag{1}$$

In the equation, W denotes arc energy, U represents arc voltage, and I stands for arc current. The fluctuation of arc energy generated during the arcing process in the experiment is depicted in Figure 5. The total energy released by the arc throughout the entire arcing process is approximately 2438 kJ, varying with changes in both arc voltage and current.

B. UHF PD SIGNALS

When a high voltage is applied between the electrodes in the arcing device, the insulating oil gap between the electrodes breaks down to form an arc channel. At a microscopic level, this phenomenon is characterized by the ionization of a large number of oil molecules near the high-voltage electrode under the influence of a high-voltage electric field, resulting in clusters of free electrons. These clusters of free electrons move at a specific velocity along the direction of the electric field towards the ground electrode where they undergo neutralization. The generation and movement of these free electron clusters are macroscopically manifested as pulsed current. Due to variations in their speed under the influence of an electric field, transient electromagnetic fields with diverse spectral characteristics are excited and emit electromagnetic waves in spherical wave form into their surroundings.

The UHF sensor utilized in this experiment incorporates the sensing unit into the transformer oil tank via a flange interface. The metal enclosed structure of the transformer oil tank effectively shields external discharge interference signals, such as corona discharges. Simultaneously, the combination of ''epoxy insulation partition + sealing ring'' ensures the hermetic sealing of the transformer oil tank body.

The UHF electromagnetic signals recorded during the arcing process are depicted in Figure 6 (a). Upon arc ignition, a high-voltage electric field between the arcing electrodes induces electromagnetic pulse signals. Within 80 ms of pressurization, the distribution of UHF electromagnetic pulses appears relatively uniform, lacking discernible phase characteristics. The overall amplitude level of UHF pulse signals during the arcing process is comparatively low. Over 4 sine wave periods, the maximum amplitudes of UHF pulses measure 53 mV, 42 mV, 46 mV, and 35 mV respectively, with minimal variation in pulse amplitude. Even after pressurization ceases, UHF signals remain detectable at a relatively stable level. Within 10 ms following the conclusion of pressurization, the maximum amplitude of UHF pulses registers at 38 mV.

C. HIGH-FREQUENCY CURRENT PD SIGNALS

The pulsed current generated by arc discharge is partially grounded through the grounding lead into the earth. The current sensor utilizes electromagnetic induction to measure the pulsed current. This paper focuses on the PD signal characteristics of arcing discharge. Accordingly, the unit 'mV' is used to characterize the strength of current signals, without converting it into current values in the unit of 'A'. In this experiment, the high-speed acquisition and processing unit of the current sensor enables rapid acquisition of raw data of pulsed current signals, while the data processing unit implements signal conditioning and frequency division-based data processing using FPGA and DSP principles.

Figure 6 (b) illustrates the current PD signal within the frequency range of 1 MHz to 30 MHz. Upon arc ignition, an intense pulse current signal is generated by the arc discharge, reaching a maximum amplitude of 717 mV for the initial cluster of signals, significantly surpassing that of UHF electromagnetic signals. Subsequently, the amplitude of the current signal rapidly diminishes. Approximately 0.39 ms into the arc discharge, the amplitude of the second cluster's current pulse signal decreases to 60 mV. The high-frequency current signals then continue to decline, with no discernible third cluster of pulse signals observed throughout the entire arc discharge process.

D. MEDIUM-FREQUENCY CURRENT PD SIGNALS

The current pulse signal within the frequency range of 10 kHz to 1 MHz, as measured during the experimental process, is depicted in Figure 6 (c). Similar to the UHF electro-magnetic signal and high-frequency current signal, the amplitude level of the medium-frequency current signal reaches its peak at arc ignition, with a maximum amplitude of 752 mV for the first cluster pulse. The overall amplitude level of the medium-frequency current signal is comparable to that of the high-frequency current signal, significantly surpassing

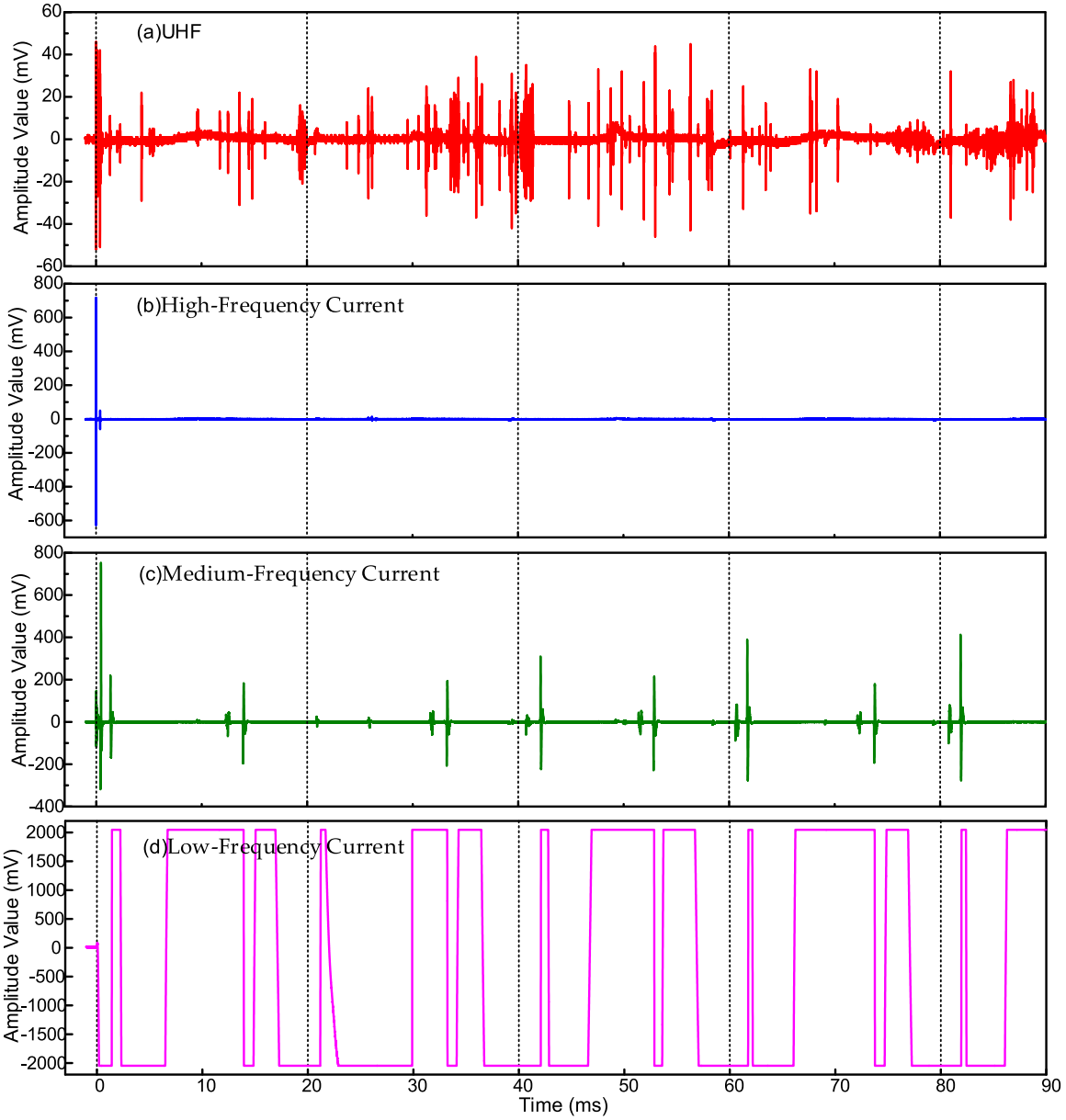

FIGURE 6. Variation of UHF electromagnetic signals and current signals during arcing process.

that of the UHF electromagnetic signal. It can be observed that, apart from the second power cycle, there are typically two clusters of current pulse signals within each power cycle. The phase distribution correlation of these pulse signals is robust and they predominantly occur during the rising phase of positive and negative half-cycles of arc voltage. Additionally, within each cycle, the amplitude value of the first cluster pulses exceeds that of second cluster pulses. Throughout continuous arc discharge, there is an overall oscillating attenuation trend in amplitude level for medium-frequency current signals. The maximum amplitudes for these signals within each cycle are 752 mV, 193 mV, 223 mV and 277 mV respectively. Furthermore, akin to UHF electromagnetic signals, medium-frequency current signals remain detectable after pressurization ends in experiments. The phase distribution remains consistent with that during pressurization.

E. LOW-FREQUENCY CURRENT PD SIGNALS

Figure 6 (d) illustrates the current signal within the frequency range of 40 Hz to 1 kHz. In contrast to the UHF electromagnetic signal, high-frequency current signal, and medium-frequency current signal, the low-frequency current signal exhibits a continuous periodic pattern. It is evident that this low-frequency current signal approximately aligns with the periodic fluctuation trend of power frequency. Furthermore, the overall amplitude level of the low-frequency current

signal is notably high, surpassing the measurement range set by sensors during arc discharge.

F. COMPARISON OF ELECTROMAGNETIC PD SIGNALS

The generation mechanisms of UHF electromagnetic signals and current signals induced by arc discharge exhibit consistency. When subjected to a high-voltage electric field, numerous oil molecules become ionized, forming clusters of free electrons that rapidly move and neutralize to create discharge pulses. A portion of these pulses generate transient electromagnetic fields in space, emitting electromagnetic waves into the surrounding environment and being detected by UHF sensors. While another portion flows to the ground through grounding wires as pulse currents and is detected by grounding current sensors [5].

Through comparison of the variations in UHF electromagnetic wave signals and current signals during the arcing process depicted in Figure 6 (a)∼(d), it is evident that the UHF electromagnetic signals and different frequency current signals exhibit distinct evolutionary patterns. The overall amplitude level of the UHF electromagnetic signal is minimal, with a relatively uniform signal distribution and no discernible phase characteristics. Following completion of experimental pressurization, continuity in the UHF signal persists, with no significant attenuation in signal amplitude observed. In contrast, the amplitude level of high-frequency current signals during arc ignition exceeds that of UHF electromagnetic signals; however, once a stable discharge channel for arc is established, there is rapid diminishment in amplitude level of high-frequency current signals. The amplitude level of medium-frequency current signals reaches its peak at the onset of arcing. Upon the establishment of an arc discharge channel, the medium-frequency current pulse signal experiences oscillation decay, resulting in an overall amplitude level equivalent to that of high-frequency current signals, significantly surpassing that of UHF electromagnetic signals. There is a strong correlation in phase distribution for medium-frequency current pulse signals, predominantly occurring during both positive and negative half-cycle voltage rise stages of arcs. Similar to UHF electromagnetic signals, the medium-frequency current signal persists after completion of the test pressure. The low-frequency current signal exhibits a continuous periodic waveform, closely mirroring the periodic fluctuations in power current. Notably, the overall amplitude level of the low-frequency current signal is the largest.

Through comparison of the amplitude levels of UHF electromagnetic signals and current signals at various frequencies, it is evident that during arcing processes, the arc signals primarily propagate outward in the form of grounding currents, with lower signal strength being radiated in the form of electromagnetic waves. Furthermore, there are significant differences in characteristics among current signals at different frequencies. Throughout the entire arcing process, current signals are predominantly concentrated in the lower frequency range, with the amplitude of low-frequency current signals consistently surpassing that of high-frequency and medium-frequency current signals. High-frequency current signals mainly manifest during the pre-penetration stage of arcing discharge channel when there is relatively high insulation strength between electrode gaps, forming a higher frequency pulse necessary for discharge. Once a stable discharge channel is established between test electrodes, the insulation strength within the gap decreases significantly and high-frequency pulses rapidly decay. The medium-frequency signal is predominantly observed during the ascending phase of both positive and negative half-cycle arc voltages, exhibiting a strong correlation with phase distribution. Following the conclusion of pressurized arcing tests, continuous monitoring of UHF electromagnetic signals, as well as medium-frequency and low-frequency current signals, remains feasible. These phenomena may be attributed to sustained discharges subsequent to pressurization, stemming from the rapid accumulation of a substantial quantity of space charges in oil insulation near electrode regions during the process of arc discharge.

G. ACOUSTIC SIGNALS

During arc discharge in oil insulation, the occurrence of current pulses is consistent. The sudden release of energy from charge neutralization and heating expansion in the discharge area results in instantaneous thermal expansion. As the pulsed current periodically decays, the heated and expanded region rapidly returns to its original state. This rapid change in volume of insulating medium space generated by the discharge pulse can produce sound waves, which propagate through spherical waves centered on the discharge area into surrounding space [22]. Furthermore, arc discharges have the potential to cause cracking and decomposition of insulating oil, leading to a significant production of gas bubbles such as acetylene and hydrogen within the discharge area. These bubbles continuously oscillate during prolonged discharges, also generating sound waves in their surroundings [23]. The fiberoptic acoustic sensor utilized in this experiment monitors acoustic signals by modulating the refractive index of fiber Bragg gratings through acoustic wave vibrations [21].

The variation of the acoustic signal recorded during the testing procedure is illustrated in Figure 7. Initially, the sensor detected a rapid change in the acoustic signal, reaching a maximum amplitude of 1580 mV. As the arc discharge continued, there was continuous fluctuation in the intensity of the acoustic signal. Around 55 ms, the amplitude decayed to near background levels before beginning to fluctuate and increase again around 60 ms. Throughout the entire arcing process, the sensor primarily captured superimposed signals including electric arc discharge, explosion-proof device activation, and transformer tank vibration. The changes in amplitude of acoustic signals provide a comprehensive representation of multiple source acoustic signal transmission and reflection.

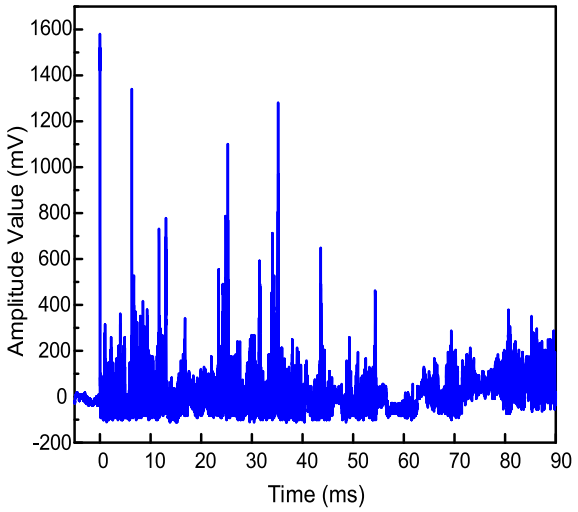

FIGURE 7. Acoustic signal variation during arcing process.

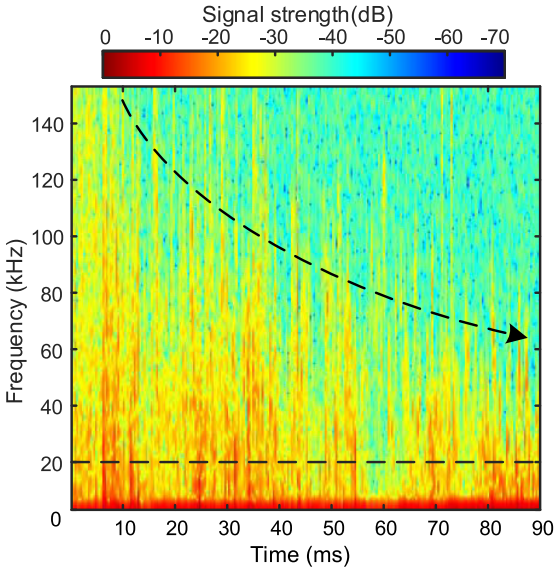

FIGURE 8. Time-frequency distribution of acoustic signals during arcing process.

The time-domain acoustic signal depicted in Figure 7 undergoes a transformation into a frequency-domain distribution, as illustrated in Figure 8. The transformation is based on the Fourier Transform, which can be readily implemented through MATLAB software. The frequency-domain distribution of the acoustic signal is predominantly concentrated within the audible frequency range below 20 kHz. During the initial phase of arc ignition, there is a relatively high intensity of high-frequency acoustic signals. As the arc discharge progresses, the frequency distribution of the acoustic signal gradually shifts towards lower frequency ranges. The intensity of high-frequency sound signals diminishes gradually, while the proportion of audible frequency range signals continues to increase.

H. PRESSURE WAVE SIGNALS

During arc discharge in the oil insulation of a transformer, the cracking and decomposition of the oil in the discharge area result in the generation of significant quantities of gases such as acetylene and hydrogen, which rapidly accumulate to form bubbles. Simultaneously, the heat produced in the discharge area causes these bubbles to expand due to heating, leading to pressure differentials and generating outward-propagating pressure waves. The fiber optic pressure sensor utilized in this experiment monitors fluctuations in pressure signals by demodulating the corresponding relationship between the wavelength of fiber Bragg grating and pressure [21].

The fluctuations in internal pressure recorded during the experiment are illustrated in Figure 9. Consistent with the principles of pressure sensor interpretation, the positive and negative values of the pressure signal indicate the relative directional relationship between the pressure wave and the sensor unit. A positive pressure signal indicates that the fiber optic sensor unit is undergoing negative pressure and stretching, while a negative value signifies that it is experiencing positive pressure and compression. The signal captured by the pressure sensor in this study reflects changes in internal transformer pressure. Upon initiation of the arc ignition test, a significant release of energy from arc discharge leads to a sudden surge in pressure, peaking at approximately 52.8 kPa around 0.2 ms. Subsequently, due to intervention by an explosion-proof device, there is a rapid decline in pressure to 7.9 kPa at 10 ms, followed by oscillation around 2.5 kPa after 40 ms. It should be noted that our experimental setup monitored peak pressures significantly lower than those generated by arcing faults within real transformers; this difference can be attributed to swift release of pressures facilitated by the explosion-proof device during testing. These findings also serve to validate the effectiveness of explosion-proof devices

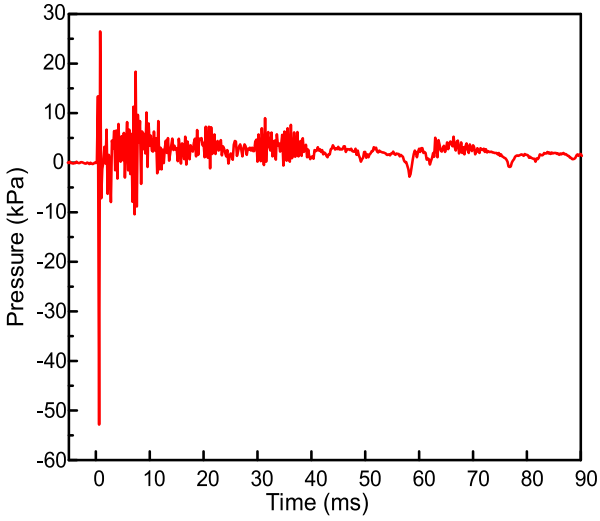

FIGURE 9. Internal pressure signal variation in transformers during arcing process.

for preventing transformer explosions. The numerical disparities between the pressure signal in this experiment and those in existing arc discharge tests [18], [19] might be associated with variations in experimental configuration, arc energy, oil tank structure, and explosion-proof device performance.

IV. CONCLUSION

Based on the arc fault test platform constructed within a real-type transformer oil tank, this study investigates the evolutionary patterns and generation mechanisms of multi-source arc signals during arc discharge faults occurring inside transformers. The primary conclusions are as follows:

1) The experiment confirmed the efficacy of the transformer fault monitoring system in detecting electrical arc discharge faults within the transformer. This system is comprised of an integrated UHF sensor, acoustic sensor, and pressure sensor, along with external grounding current sensors.

2) The test results have bridged the gap in the investigation of the evolutionary pattern of arc signals in arcing faults in transformers. Throughout the arcing process, there is a relatively uniform phase distribution of UHF electromagnetic signals with a lower overall amplitude; the high-frequency current signal experiences rapid decay following arc initiation; medium-frequency current signals exhibit obvious phase distribution correlation and signal continuity; and low-frequency current signals manifest as continuous periodic signals.

3) The characteristic signal evolution of arcing faults exhibits significant divergence from that of partial discharge faults in transformers. The pulse signals generated by arc discharges predominantly propagate in the form of grounding currents, with relatively low amplitudes of UHF electromagnetic signals; acoustic and pressure signals manifest higher amplitudes during arcing faults, which is correlated to the expansion of a substantial volume of gas produced by arc discharges.

4) By analyzing various discharge signal features from multiple sources, it is feasible to accurately detect internal arcing faults in transformers and promptly mitigate the risk of transformer explosion incidents.

REFERENCES

[1] J. Li, X. Han, Z. Liu, and Y. Li, "Review on partial discharge measurement technology of electrical equipment," *High Voltage Eng.*, vol. 41, no. 8, pp. 2583–2601, Aug. 2015.

[2] B. Qi, Z. Wei, C. Li, X. Zhang, M. Yu, and J. Zuo, "Development of discharge of internal gas-gap defect in oil-paper insulation under AC and DC combined voltage," *Proc. CSEE*, vol. 34, no. 36, pp. 6554–6561, Dec. 2014.

[3] Y. Jia, S. Ji, J. Li, S. Jia, X. Luo, K. Wang, and J. Sun, "Overview on the characteristics of power frequency Arc in transformer oil and transformer explosion protection," *Proc. CSEE*, vol. 44, no. 7, pp. 2910–2926, Dec. 2024.

[4] M. D. Judd, O. Farish, J. S. Pearson, T. Breckenridge, and B. M. Pryor, "Power transformer monitoring using UHF sensors: Installation and testing," in *Proc. Conf. Rec. IEEE Int. Symp. Electr. Insul.*, Anaheim, CA, USA, Apr. 2000, pp. 373–376.

[5] M. D. Judd, "Dielectric windows improve sensitivity of partial discharge detection at UHF," in *Proc. Conf. Rec. IEEE Int. Symp. Electr. Insul.*, Anaheim, CA, USA, Apr. 2000, pp. 304–307.

[6] S. Liu, C. Wang, and L. Du, "UHF signals calibration for typical partial discharge defects in transformer oil," *High Voltage Eng.*, vol. 43, no. 9, pp. 2983–2990, Sep. 2017.

[7] Z. Tang, C. Wang, J. Chen, W. Wu, and C. Li, "Pulse interferences elimination and classification of on-line UHF PD signals," *High Voltage Eng.*, vol. 35, no. 5, pp. 1026–1031, May 2009.

[8] H. Wang, "The evolution process of typical partial discharges in oil-paper insulation transformers," Ph.D. dissertation, North China Electr. Power Univ., Beijing, China, 2010.

[9] H.-Y. Zhou, G.-M. Ma, M. Zhang, H.-C. Zhang, and C.-R. Li, "A high sensitivity optical fiber interferometer sensor for acoustic emission detection of partial discharge in power transformer," *IEEE Sensors J.*, vol. 21, no. 1, pp. 24–32, Jan. 2021.

[10] R. Shi, S. Wang, G. Ma, Q. Weiqi, J. Hu, X. Zhang, H. Zhou, and S. Gao, "optical fiber ultrasonic sensing for partial discharge based on acoustic focusing structure," *Proc. CSEE*, vol. 43, no. 21, pp. 8518–8527, Nov. 2023.

[11] J. Qiao, W. Zhang, Q. Shao, and H. Zhao, "Long distance detection technology for transformer partial discharge based on linear cavity fiber laser," *Proc. CSEE*, vol. 43, no. 15, pp. 6145–6155, Aug. 2023.

[12] Z. Zhang, J. Lei, W. Chen, C. Wei, K. Wu, and Y. Xiangshi, "Transformer's partial discharge and oil temperature sensing method based on multi-parameter fiber optic F-P sensing," *High Voltage Eng.*, vol. 48, no. 1, pp. 58–65, Jan. 2022.

[13] H.-Y. Zhou, G.-M. Ma, W.-Q. Qin, M. Zhang, Q. Zhang, Z.-Q. Lin, and J. Jiang, "A multiplexing optical partial discharge sensing system for power transformer using a single photodetector," *IEEE Trans. Power Del.*, vol. 36, no. 3, pp. 1911–1913, Jun. 2021.

[14] R. Shi, Z. Lin, W. Qin, J. Hu, H. Zhou, S. Gao, and S. Gao, "Partial discharge acoustic emission detection and localization based on active fiber grating array," *Proc. CSEE*, vol. 43, no. 1, pp. 358–368, Jan. 2023.

[15] C. Shi, G. Ma, N. Mao, Q. Zhang, C. Li, Z. Li, and H. Wang, "study on fiber ultrasonic location technology of partial discharge in transformer based on wavelength division multiplexing/time-division multiplexing technology," *Proc. CSEE*, vol. 37, no. 16, pp. 4873–4879, Aug. 2017.

[16] L. Yang, R. Liao, C. Sun, and K. Wang, "Partial discharge characteristics and risk assessment method for oil-paper," *Proc. CSEE*, vol. 31, no. 1, pp. 123–130, Jan. 2011.

[17] J. Zhou, "Research on partial discharge characteristics and feature extraction of suspended particles in oil," Ph.D. dissertation, Chongqing Univ., Chongqing, China, 2012.

[18] Z. Chong, L. Lu, Y. Zhou, J. Wu, Y. Liu, and Y. Li, "Effect on pressure generation characteristics by Arc in oil-filled closed tank," *High Voltage Eng.*, vol. 49, no. 9, pp. 3887–3897, Sep. 2023.

[19] Z. Liu, L. Lu, Y. Zhou, Z. Chong, D. Hu, and Y. Li, "Research on pressure characteristics of AC turret on Arc fault," *Proc. CSEE*, vol. 41, no. 13, pp. 4688–4698, Jul. 2021.

[20] *IEEE Standard for Overhead-Type Distribution Transformers 500 KVA and Smaller: High Voltage, 34 500 V and Below; Low Voltage, 7970/13 800Y V and Below*, IEEE Standard C57.12.20-2011, 2011.

[21] J. Mao, H. Meng, Z. Yuping, B. Qi, H. Teng, W. Zheng, S. Pan, and C. Li, "High sensitive pressure optical sensing method adapted to transformer internal environment," *Proc. CSEE*, vol. 42, no. 10, pp. 3826–3836, May 2022.

[22] T. Boczar, "Identification of a specific type of PD from acoustic emission frequency spectra," *IEEE Trans. Dielectr. Elect. Insul.*, vol. 8, no. 4, pp. 598–606, Aug. 2001.

[23] D.-J. Kweon, S.-B. Chin, H.-R. Kwak, J.-C. Kim, and K.-B. Song, "The analysis of ultrasonic signals by partial discharge and noise from the transformer," *IEEE Trans. Power Del.*, vol. 20, no. 3, pp. 1976–1983, Jul. 2005.

CHENLEI HAN received the Ph.D. degree in electrical engineering from Tianjin University, China, in 2021. He is currently a Postdoctoral Researcher with China Electric Power Research Institute (CEPRI). His research interests include transformer condition monitoring and insulation degradation assessment.

KELI GAO received the B.S. and M.S. degrees in electrical engineering from Xi'an Jiaotong University. Currently, he is the General Manager of CEPRI and the Director of the High Voltage Committee of the Chinese Society of Electrical Engineering (CSEE). He is mainly engaged in the research of safe operation technology for power transmission systems, transformation equipment and ultra-high voltage transmission technology, and the SF6 alternative technology.

WENZHI CHANG received the Ph.D. degree in high voltage and insulation from North China Electric Power University, Beijing, China, in 2013. He is currently a Senior Engineer with CEPRI. His research interest includes condition monitoring of power apparatus.

BO QI received the Ph.D. degree in high voltage and insulation from North China Electric Power University, Beijing, China, in 2010. He is currently a Professor with the School of Electric and Electronic Engineering, North China Electric Power University. His current research interests include electrical insulation and condition monitoring of power apparatus.

JIANGANG BI received the B.S. and M.S. degrees in electrical engineering from Xi'an Jiaotong University. He is currently a Senior Engineer with CEPRI. His research interest includes condition monitoring of power apparatus.

SHUAI YUAN received the Ph.D. degree in electrical engineering from Harbin Institute of Technology, China, in 2010. He is currently a Senior Engineer with CEPRI. His research interest includes online monitoring for dissolved gases in oil.

MENG HUANG received the Ph.D. degree in electrical engineering from Tsinghua University, Beijing, China, in 2016. He is currently an Associate Professor with the School of Electric and Electronic Engineering, North China Electric Power University. His current research interests include electrical insulation, condition monitoring of power apparatus, and space charge measurement.

TINGYU GAO received the M.S. degree in high voltage and insulation from North China Electric Power University, Beijing, China, in 2023. She is currently an Engineer with CEPRI. Her research interest includes online monitoring of power equipment.